Filtering and Segmentation of Polarimetric SAR Data Based on Binary Partition Trees

Alberto Alonso-González, Carlos López-Martínez, *Senior Member, IEEE*, and Philippe Salembier, *Fellow, IEEE*

***Abstract*—In this paper,we propose the use of binary partition trees (BPT) to introduce a novel region-based and multi-scale polarimetric SAR (PolSAR) data representation. The BPT structure represents homogeneous regions in the data at different detail levels. The construction process of the BPT is based, firstly, on a region model able to represent the homogeneous areas, and, secondly, on a dissimilarity measure in order to identify similar areas and define the merging sequence. Depending on the final application, a BPT pruning strategy needs to be introduced. In this paper, we focus on the application of BPT PolSAR data representation for speckle noise filtering and data segmentation on the basis of the Gaussian hypothesis, where the average covariance or coherency matrices are considered as a region model. We introduce and quantitatively analyze different dissimilarity measures. In this case, and with the objective to be sensitive to the complete polarimetric information under the Gaussian hypothesis, dissimilarity measures considering the complete covariance or coherency matrices are employed. When confronted to PolSAR speckle filtering, two pruning strategies are detailed and evaluated. As presented, the BPT PolSAR speckle filter defined filters data according to the complete polarimetric information. As shown, this novel filtering approach is able to achieve very strong filtering while preserving the spatial resolution and the polarimetric information. Finally, the BPT representation structure is employed for high spatial resolution image segmentation applied to coastline detection. The analyses detailed in this work are based on simulated, as well as on real PolSAR data acquired by the ESAR system of DLR and the RADARSAT-2 system.**

***Index Terms*—Binary partition tree (BPT), polarimetry, segmentation, speckle filtering, synthetic aperture radar.**

I. Introduction

SAR polarimetry (PolSAR) has demonstrated, particularly during the last decade, its significance for the analysis and the characterization of the earth surface, as well as for the quantitative retrieval of biophysical and geophysical parameters. The capability to explore the complete space of polarization states represents one of the most important properties of PolSAR data, as optimization procedures may be foreseen [1]. The second important property of PolSAR data is its inherent multidimensional nature that allows a more precise characterization of the scattering process at the resolution cell than single polarization data and, eventually, a better characterization of the scatter or scatters within that resolution cell.

Manuscript received October 15, 2010; revised March 23, 2011; accepted June 12, 2011. Date of publication August 4, 2011; date of current version January 20, 2012. This work has been supported by the Spanish MICINN project TEC2008-06764-C02-01 and the CUR of the DIUE of the Autonomous Government of Catalonia and the European Social Fund.

The authors are with the Department of Signal Theory and Communications, Technical University of Catalonia, 08034 Barcelona, Spain (e-mail: alberto.alons@gmail.com; carlos.lopez@tsc.upc.edu; philippe.salembier@upc.edu).

Digital Object Identifier 10.1109/TGRS.2011.2160647

As a consequence of the coherent recording and processing of the scattered radar echoes, SAR systems are able to generate complex, high spatial resolution images of the observed area, independent of the day–night cycle and with little influence of atmospheric effects. The complex nature of SAR data, together with the fact that the scattering process in the resolution cell may be due to a certain number of elementary echoes, is on the origin of the speckle term. Despite speckle is determined by the scattering process itself, its complexity makes necessary to consider it from a stochastic point of view and then, to assume speckle as a noise term. The characterization of speckle noise must be carefully addressed, particularly for PolSAR data, taking into account the nature of the scatters within the resolution cell. In the case of point scatters, as the scattered signal is only due to this single scatter, recorded data are speckle free, and the value of the signal itself may be employed to characterize the scattering process and the scatter itself. For distributed scatters, speckle is said to be fully developed in the sense that it is produced from the coherent addition of a large number of individual echoes produced by the individual scatters in the resolution cell. Consequently, in the later case, the information to retrieve refers to the necessary knowledge to specify completely the probability density distribution (pdf) of the acquired PolSAR data. This information must be estimated from the recorded SAR data. In other words, speckle should be filtered from data to grant access to the information of interest.

SAR and PolSAR data are nonstationary as they reflect the complexity of the environment. Assuming that all the stochastic processes involved in the filtering process are ergodic, PolSAR filters must adapt to this nonstationarity. Most of the PolSAR speckle filters presented in the literature deal with nonstationarity by considering locally stationary data. Based on this hypothesis, two major questions arise. On the one hand, the statistical model or pdf under which stationarity shall be defined and, on the other hand, the range of this stationarity. With respect to the statistical model, most of the filtering techniques, but also most of the techniques focused on the extraction of quantitative physical parameters, consider the multidimensional complex Gaussian speckle noise model. Under this hypothesis, the covariance, as well as the equivalent coherency or Muëller matrices, represent the most important radar observables, in which maximum likelihood estimation (MLE) is the well-known boxcar or multilook filter. This filter privileges estimation accuracy at the cost of spatial resolution. However, the previous assumption of locally stationary data may be violated resulting in a loss of spatial resolution or a mixture of nonhomogeneous areas. With the aim to avoid the breaking of the assumption

of locally stationary data, a linear minimum mean square error (LMMSE) approach has been proposed in [3] where local statistics are estimated on the basis of edge aligned windows. This idea has been pursued in [4], where an adaptive neighborhood is constructed for every single pixel of the image, taking into account the statistical properties of the pixel itself.

Despite the techniques presented in [3] and [4] have been proved to result into a proper filtering, several questions must be answered in order to finally determine the filtering capabilities. One of the major concerns of the previous approaches is the way they determine local stationarity. On the basis of the Gaussian hypothesis, local stationarity is analyzed only in terms of the diagonal elements of the covariance matrix. Hence, they do not take into account the correlation information determined by the off-diagonal elements of the covariance matrix, despite it has been shown that if considered, optimized filtering capabilities result [5]. In addition, the way local neighbors are obtained in [4] does not guarantee that adjacent and stationary pixels result into the same local area of influence. A final aspect that must be also considered with respect to the estimation of physical information is that a minimum amount of independent samples is mandatory to secure a correct estimation of the information of interest [6].

In order to tackle these issues, we propose the use of binary partition trees (BPT) [7], [22]. The BPT is an image representation that is region based and multi-scale. The leaf nodes of the tree represent the pixels in the original image, whereas the remaining nodes represent regions that are obtained by the merging of the two neighboring regions represented by two child nodes. The root node corresponds to the entire image. The BPT can represent nonstationary signals because it is region based, that is, each region can represent a locally stationary part of the signal. Moreover, it is a multi-scale representation allowing, at the same time, the description of very local information, thanks to the nodes close the tree leaves, and the description of global behavior, thanks to the nodes close to the tree root, as these nodes represent very large regions. In order to construct and to analyze the BPT in the context of applications, the tree nodes have to be described. An interesting feature of the BPT approach is its flexibility in the sense that it is not restricted to any particular model. In the case of PolSAR data, virtually any model representing the polarimetric information can be used. As it can be seen, the BPT can be considered as a first abstraction step with respect to the original image. The processing strategy involves, therefore, first, a tree construction and, then, a tree pruning to extract either a simplified image for filtering applications or a partition for classification or segmentation applications.

The organization of this paper is as follows: Section II reviews the main characteristics of the PolSAR data and discusses its representation and processing with BPT. Section III analyzes in detail the tree construction process and focuses in particular on the definition of the similarity between regions used to define the merging order. Once the BPT has been computed, it can be used for many applications. In this paper, we discuss filtering application in Section IV as well as a specific segmentation application in Section V. Finally, Section VI presents the conclusions.

II. Processing PolSAR Data With BPT

A. SAR Polarimetry

A PolSAR system measures, for every resolution cell, the scattering matrix $\mathbf{S}$. By means of the lexicographic orthogonal basis for 2×2 complex matrices [2], and considering the backscattering direction under the backscattering alignment convention, $\mathbf{S}$ leads to the target vector $\mathbf{k}$

$$\mathbf{k} = [S_{hh}, \sqrt{2}S_{hv}, S_{vv}]^T \tag{1}$$

where h and v denote the horizontal and vertical wave polarization states, respectively and ^{T} indicates vector transposition. In those cases in which the resolution cell contains only one scatter, or its scattering is largely dominated by a principal one, (1) characterizes completely the scattering process in the resolution, that is, (1) may be employed to characterize the target under study. When the resolution cell contains a certain number of single scatters, (1) corresponds to a coherent combination of the different contributions of this set of single scatters. This combination process receives the name of speckle. As indicated previously, speckle must be considered as a noise term. Under this hypothesis, the information of interest acquires sense only from a stochastic point of view, that is, this information refers to the set of parameters necessary to determine completely the pdf of (1).

The statistical characterization of (1) in case of distributed scatters involves the introduction of a particular pdf to describe its stochastic nature. This process is normally performed under certain simplifying approximations. Under the assumption that the return from a particular resolution cell is due to the coherent addition of the returns from a large number of individual scatters, none of which is dominant, the Central Limit Theorem applies [8], and $\mathbf{k}$ is distributed according to a multidimensional, zero-mean, complex Gaussian pdf

$$p_{\mathbf{k}}(\mathbf{k}) = \frac{1}{\pi^3 |\mathbf{C}|} \exp(-\mathbf{k}^H \mathbf{C}^{-1} \mathbf{k}) \tag{2}$$

where ^{H} is the complex conjugate transpose of a vector and $\mathbf{C}$ represents the covariance matrix

$$\begin{aligned} \mathbf{C} &= E\{\mathbf{k}\mathbf{k}^H\} \\ &= \begin{bmatrix} E\left\{S_{hh}S_{hh}^H\right\} & \sqrt{2}E\left\{S_{hh}S_{hv}^H\right\} & E\left\{S_{hh}S_{vv}^H\right\} \\ \sqrt{2}E\left\{S_{hv}S_{hh}^H\right\} & 2E\left\{S_{hv}S_{hv}^H\right\} & \sqrt{2}E\left\{S_{hv}S_{vv}^H\right\} \\ E\left\{S_{vv}S_{hh}^H\right\} & \sqrt{2}E\left\{S_{vv}S_{hv}^H\right\} & E\left\{S_{vv}S_{vv}^H\right\} \end{bmatrix} \end{aligned} \tag{3}$$

where $E\{x\}$ indicates the statistical expectation of the stochastic process x. It is clear that the approximations that led to (2) will limit its range of applications. Hence, (2) is usually considered as a multidimensional SAR signal model for homogeneous areas. Equation (2) is not able to describe, for instance, textured scenarios. In these cases, it is necessary to increase the complexity of the statistical model in order to accommodate the texture information.

The MLE of $\mathbf{C}$, i.e., the multilook, under the assumption of statistical ergodicity and homogeneity, is obtained by

substituting the statistical expectation by a spatial averaging

$$\mathbf{Z} = \langle \mathbf{k}\mathbf{k}^H \rangle_n = \frac{1}{n}\sum_{i=1}^{n} \mathbf{k}_i \mathbf{k}_i^H \tag{4}$$

where n indicates the number of independent looks or samples employed to estimate $\mathbf{C}$ and $\mathbf{k}_i$ corresponds to the target vector of the ith sample. The estimated covariance matrix $\mathbf{Z}$ receives the name of the sample covariance matrix, which is statistically determined by the Wishart distribution [9]–[11]

$$p_{\mathbf{Z}}(\mathbf{Z}) = \frac{n^{3n}|\mathbf{Z}|^{n-3}}{|\mathbf{C}|^n \widetilde{\Gamma}_3(n)} \text{etr}(-n\mathbf{C}^{-1}\mathbf{Z}) \tag{5}$$

where $\text{etr}(\mathbf{X})$ is the exponential of the matrix trace and

$$\widetilde{\Gamma}_3(n) = \pi^3 \prod_{i=1}^{3} \Gamma(n-i+1). \tag{6}$$

As given in (4), $\mathbf{C}$ is estimated from a finite number of samples n. Note that (5) is only valid if $\mathbf{Z}$ is a full rank matrix, which implies $n \geq 3$, otherwise, the Wishart distribution cannot be defined. Since the estimated covariance matrix $\mathbf{Z}$ is itself a multivariate random variable, it will present an error with respect to the value to recover, i.e., $\mathbf{C}$. This error might be considered as being produced by a noise component. The advantage of such a characterization is that an optimized filtering might be envisaged.

B. BPT Computation and Processing Strategy

We propose to tackle a large number of applications related to PolSAR data by performing initially a first step of abstraction from the original pixel-based representation of the image. This abstraction step is done through the computation of a BPT and should be as generic or application independent as possible. Once the BPT has been computed, its nodes are characterized and analyzed depending on the application of interest and the final result can generally be obtained through an application-dependent tree pruning.

In order to be able to construct the BPT structure in an efficient manner, it would be interesting to decompose the process into simple steps, making possible to tackle the process with an iterative algorithm. In this sense, the BPT construction process may be viewed as the introduction of all the hierarchical division–fusion relationships between the image pixels. Hence, this process can be decomposed in the inclusion of each hierarchical relationship, so the tree structure can be constructed iteratively computing one new division–fusion relationship between nodes per step.

In order to construct the BPT structure, there are two main approaches:

1) One focused on division or *top-down* approach: In each construction process step, a new division relationship is added to the structure, so a selected region of the image is separated into two connected and mutually disjoint regions that will become the two child nodes of the one containing the selected region.
2) One focused on fusion or *bottom-up* approach: Another conceptualization of the construction process is to add a fusion relationship between two neighboring regions of the image at each step. The merging of these two zones will produce a new bigger connected region represented by their parent node.

For computational reasons, it is more feasible to address a *bottom-up tree construction* algorithm, since the number of possible new fusion relationships is more reasonable than the number of possible new divisions for a given construction step.

The BPT should be created in such a way that the most interesting or useful regions are represented. However, a possible solution, suitable for a large number of cases, is to create the tree by keeping track of the merging steps performed by a segmentation algorithm based on region merging, see [12], [13] for example. In the following, this information is referred to as the *merging sequence*. Starting from the initial partition, where each pixel is considered as an individual region, the algorithm merges neighboring regions following a similarity criterion until a single region is obtained.

To completely define the merging algorithm, one has to specify the region model and the merging order. The region model defines precisely how the set of pixels included in the regions are represented. As mentioned in the introduction, almost any model can be employed to represent polarimetric data. In this paper, we will use the average covariance matrix of the pixels included within the region as the region model, then assuming data to be distributed according to 2. The merging order defines the order in which pairs of neighboring regions are merged. In essence, this criterion should assess the similarity between regions. Section III will propose, discuss, and evaluate various families of criteria suitable for PolSAR data.

Once the tree has been computed, it can be processed or simplified by a pruning algorithm. This step is application dependent. Assume, for example, that we would like to filter the image to reduce the presence of noise. Then, the pruning should remove portions of the tree branches that are close to the original tree leaves in order to preserve as much as possible the image details. By contrast, if the application is based on segmenting or classifying the image, the pruning strategy should analyze each node of the tree looking for relevant segmentation or classification features, and the resulting pruning may be much more severe. These cases will be analyzed, respectively in Sections IV and V, respectively.

An illustration of the construction process is given in Fig. 1. The original 2×2 image involves four pixels: A, B, C, and D. They are considered as initial regions and are represented as tree leaves. The algorithm merges the four regions in three steps. In the first step, the pair of most similar regions, A and B for example, are merged and create region E. Of course, once E is created, its similarity with respect to its neighboring regions should be evaluated. Assume that after this evaluation, the pair of most similar regions are D and E. They are merged creating region F. Finally, region C is merged with region F, and this creates a region corresponding to the region of support of the whole image. In this example, the merging sequence

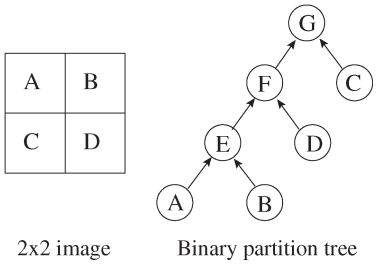

Fig. 1. Illustration of the BPT construction.

is: $(\{A, B, C, D\}, (A, B)|(D, E)|(C, F))$. This merging sequence defines the BPT as shown in Fig. 1.

III. Merging Criteria for BPT Construction for PolSAR Data

A. Merging Criteria and Dissimilarity Measures

As stated in Section II, the merging sequence determines the BPT construction. Since this process is performed iteratively, a *merging criterion* must be included in the construction process step in order to select the best fusion to perform among all the possible ones. The proposed criterion in Section II is to merge the pair of most similar regions.

In order to evaluate the similarity between regions, a measure has to be defined in the region model space. Actually, any distance in the region model space may be employed. However, other measures than distances can be used, and the more general concept of *dissimilarity measure* will be employed in the following. Mathematically, a dissimilarity measure d is similar to a distance in concept, but it has less restrictive properties [17]:

1) $d(A, B) \geq d_0$ (generalized non-negativity)
2) $d(A, B) = d_0 \Leftrightarrow A = B$ (identity)
3) $d(A, B) = d(B, A)$ (symmetry)

where A and B are two region models and d_0 represents the absolute minimum value of the dissimilarity function d. Traditionally, as explained in Section II, in PolSAR, the estimated covariance $\mathbf{C}$ or coherency $\mathbf{T}$ matrices are employed to characterize the scattering process over an homogeneous region, as defined in (4), then they may be employed as a region model in the BPT nodes.

In this context, the measure d establishes the similarity between each pair of adjacent regions. At each construction step, the two adjacent nodes with the lowest dissimilarity value are merged. Then, two dissimilarity measures d_1 and d_2 are equivalent if they define the same merging sequence. As a consequence, any monotonic function of the dissimilarity measure will lead to the same merging sequence, and then it will produce the same BPT representation.

B. Dissimilarity Measures

In this paper, five dissimilarity measures are proposed and analyzed for the BPT construction process. These measures are based on two region features: the polarimetric information, contained in the $\mathbf{Z}$ matrix, as defined in (4), and the region size. Nevertheless, more complex region models and the corresponding dissimilarity measures between them can be defined.

The proposed dissimilarity measures have been classified into two different groups: those using only the information contained in the diagonal elements of $\mathbf{Z}$, and those using the full estimated covariance matrix.

1) Dissimilarity Measures Using Full $\mathbf{Z}$ *Information:* These measures consider all the information contained in the estimated covariance matrix $\mathbf{Z}$ and thus require a complete characterization of the matrix. Note that this fact will induce the need for an initial filtering in order to get full rank matrices, as seen in (5). The dissimilarities are defined between two regions, X and Y, with average covariance matrices $\mathbf{Z}_X$ and $\mathbf{Z}_Y$ and sizes of n_x and n_y pixels, respectively.

- *Symmetric revised Wishart dissimilarity* (RW). The revised Wishart dissimilarity measure was defined in [15], and it is based on a statistical test assuming that the two regions follow a Wishart pdf and that one pdf is known. Thus, it is not symmetric as it depends on which region pdf is assumed to be known. In order to generate a dissimilarity measure, a modified symmetric version is proposed using $d_s(X, Y) = d(X, Y) + d(Y, X)$ and multiplying by the region size term

$$d_{RW}(X,Y) = \left(\mathrm{tr}\left(\mathbf{Z}_X^{-1}\mathbf{Z}_Y\right) + \mathrm{tr}\left(\mathbf{Z}_Y^{-1}\mathbf{Z}_X\right)\right) \cdot (n_x + n_y) \quad (7)$$

  where $\mathrm{tr}(\mathbf{A})$ denotes the trace of the $\mathbf{A}$ matrix and $\mathbf{A}^{-1}$ its inverse.
- *Ward relative dissimilarity* (WR). In Ward hierarchical clustering [16], a measure based on the error sum-of-squares was introduced in order to quantify the information loss when two clusters are joined. The same measure can be employed as the information loss of merging two neighboring regions. However, due to the multiplicative nature of the speckle noise, a modified relative version is proposed including a normalization matrix. The Ward relative dissimilarity d_{WR} (8) is then defined as

$$d_{WR}(X,Y) = n_x \cdot \left\|\mathbf{N}_{XY}^H(\mathbf{Z}_X - \mathbf{Z}_{XY})\mathbf{N}_{XY}\right\|_F^2 + n_y \cdot \left\|\mathbf{N}_{XY}^H(\mathbf{Z}_Y - \mathbf{Z}_{XY})\mathbf{N}_{XY}\right\|_F^2 \quad (8)$$

  where $\mathbf{Z}_{XY}$ denotes the average matrix of the region $X \cup Y$, $\mathbf{A}^H$ denotes matrix $\mathbf{A}$ Hermitian transpose, $\mathbf{N}_A$ denotes the normalization matrix of $\mathbf{Z}_A$, defined as

$$\mathbf{N}_A = \begin{pmatrix} \sqrt{Z_{A_{11}}} & 0 & 0 \\ 0 & \sqrt{Z_{A_{22}}} & 0 \\ 0 & 0 & \sqrt{Z_{A_{33}}} \end{pmatrix} \quad (9)$$

  and $\|\mathbf{A}\|_F$ denotes the Frobenius matrix norm.

2) Dissimilarity Measures Using Diagonal $\mathbf{Z}$ *Elements:* These measures only employ the diagonal elements of the estimated covariance matrix $\mathbf{Z}$, corresponding to the power received at each polarization component. Consequently, they do not require any initial filtering, but they are not sensitive to the off-diagonal components of the covariance or coherency matrices.

- *Diagonal relative normalized dissimilarity* (DN) is based on the euclidean norm of the normalized difference of the diagonal vector. The difference of the diagonal vectors is

normalized by their sum, which results in a value bounded in the interval $[-1, 1]$ for each diagonal element. The dissimilarity measure is obtained computing the euclidean norm of the resulting vector and multiplying the resulting value by the sum of region sizes, as denoted in

$$d_{DN}(X,Y)=\left(\sum_{i=1}^{3}\left(\frac{Z_{X_{ii}}-Z_{Y_{ii}}}{Z_{X_{ii}}+Z_{Y_{ii}}}\right)^2\right)^{1/2}\cdot(n_x+n_y) \quad (10)$$

where A_{ij} is the index notation for the (i,j)th element of matrix $\mathbf{A}$.

- *Diagonal relative dissimilarity* (DR) is computed as the euclidean norm of the sum of relative errors between the diagonal elements multiplied by the size of the $X \bigcup Y$ region. Note that this dissimilarity measure d_{DR} (11) is not bounded, as opposite of d_{DN} (10) because the value interval of the resulting vector is open $[0,\infty)$

$$\begin{aligned} d_{DR}(X,Y)&=\left(\sum_{i=1}^{3}\left(\frac{Z_{X_{ii}}-Z_{Y_{ii}}}{Z_{Y_{ii}}}+\frac{Z_{Y_{ii}}-Z_{X_{ii}}}{Z_{X_{ii}}}\right)^2\right)^{1/2}\\ &\quad\cdot(n_x+n_y)\\ &=\left(\sum_{i=1}^{3}\left(\frac{(Z_{X_{ii}}-Z_{Y_{ii}})^2}{Z_{X_{ii}}Z_{Y_{ii}}}\right)^2\right)^{1/2}\cdot(n_x+n_y). \quad (11)\end{aligned}$$

- *Diagonal revised Wishart dissimilarity* (DW) is based on the symmetric revised Wishart dissimilarity as it is defined in (7), but only considering the diagonal elements and setting all off-diagonal elements to 0, which simplifies the matrix inversion as being the inverse of the diagonal elements. After some mathematic simplifications, it can be expressed as

$$d_{DW}(X,Y)=\left(\sum_{i=1}^{3}\left(\frac{Z_{X_{ii}}^2+Z_{Y_{ii}}^2}{Z_{X_{ii}}Z_{Y_{ii}}}\right)\right)\cdot(n_x+n_y). \quad (12)$$

The objective of the previous division among distances will be to focus specifically on the analysis of the effects of considering the off-diagonal elements of the covariance and coherency matrices when processing PolSAR data under the Gaussian assumption. Additionally, it would be possible to determine and to establish those conditions that a distance should fulfill to perform a correct processing of PolSAR data, for speckle filtering or for any other different application. First of all, the distances should be invariant under similarity transformations of the special unitary group of matrices. For example, the approach followed by [3] would be congruent with this condition, since Span is invariant under these transformations. The distance function employed in [4] and the dissimilarity measures that consider only diagonal elements would not fulfill such a condition since only diagonal elements are considered. In this sense, only the distance d_{RW} would be invariant. Nevertheless, the invariance property is not sufficient to perform a correct processing of PolSAR data. A clear example is the approach in [3]. Despite this technique is invariant under similarity transformations, it is not sensitive to the off-diagonal information. Consequently, suitable distances, apart from being invariant under similarity transformations, should consider all the information provided by the covariance and coherency matrices, as for instance the d_{RW} distance.

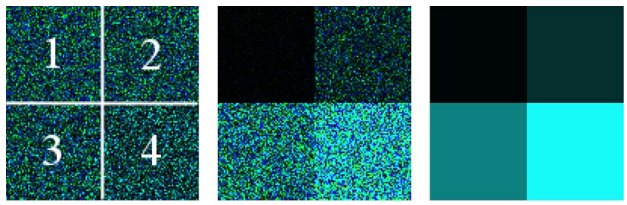

Fig. 2. Simulated PolSAR images with four equal size zones. C_{11}, C_{22}, and C_{33} are assigned to blue, red, and green channels. a) Zones shape and numeration, b) and c) one realization of the image with intensity variations and image ground truth, respectively.

IV. BPT Pruning for PolSAR Data Filtering

As described in [7], the BPT is a very attractive representation since it proposes a reduced number of regions which are assumed to be the most homogeneous at different scales. This idea can be exploited to develop PolSAR advanced speckle noise filtering. The main purpose is to obtain a subset Θ of meaningful nodes, from the tree representing homogeneous regions, which can be used to have a better estimation of the region covariance matrix (4) maintaining the image spatial resolution. This process consisting of a selection of a subset Θ of nodes from the BPT is called *BPT pruning*.

In this section, two main strategies for tree pruning focused on PolSAR speckle filtering are discussed: pruning based on the number of regions and pruning based on the region homogeneity.

A. Pruning Based on the Number of Regions

One of the simplest possible tree pruning strategies is to select the set Θ as a fixed number n_r of regions, corresponding to the most different regions of the tree. If the difference between regions is evaluated using the same dissimilarity measure used for the BPT construction process, then it is equivalent to stop the construction process when n_r regions are achieved. At that point, an image segmentation with the n_r most different regions, in terms of the employed dissimilarity measure, is obtained. Finally, the filtered image is obtained by representing all pixels within each region with the mean covariance matrix, which corresponds to the region model. In the following, this process will be called *BPT pruning based on the number of regions*.

For a quantitative evaluation of this filtering process, a simulated 128 $\times$ 128 pixels PolSAR image is proposed in Fig. 2 with four square regions of equal size. Simulated data have been generated using the complex Gaussian polarimetric model presented in [14], assuming a reflection symmetric target since most of natural targets follow this model, with covariance matrix $\mathbf{C}$ of the form

$$\mathbf{C}=\sigma_{HH}\begin{pmatrix}1 & 0 & \rho\sqrt{\gamma}\\ 0 & \varepsilon & 0\\ \rho^*\sqrt{\gamma} & 0 & \gamma\end{pmatrix} \quad (13)$$

where * denotes complex conjugate.

Three sets of images have been simulated according to (13) with $\gamma_i = 1$ and $\varepsilon_i = 0.1$ and variations for σ_{HHi} and ρ_i in different regions $i = 1, \ldots, 4$ as denoted in Fig. 2(a).

1) Variations in intensity: $\rho_i = 0.5$; $\sigma_{HH} = \{1, 9, 25, 49\}$.
2) Variations in correlation: $\rho = \{0, 0.25e^{j\pi}, -0.5, 0.75e^{-j\pi}\}$; $\sigma_{HHi} = 1$.
3) Variations both in correlation and in intensity: $\rho = \{0, 0.25e^{j\pi}, -0.5, 0.75e^{-j\pi}\}$; $\sigma_{HH} = \{1, 9, 25, 49\}$.

A matrix relative error measure is also proposed in order to asses quantitatively the goodness of the processed image X in comparison with the ground truth Y

$$E_R(X, Y) = \frac{1}{n_h \cdot n_w} \sum_{i=1}^{n_h} \sum_{j=1}^{n_w} \frac{\|\mathbf{X}^{ij} - \mathbf{Y}^{ij}\|_F}{\|\mathbf{Y}^{ij}\|_F} \qquad (14)$$

where n_h and n_w are the image height and width in pixels, respectively, $\mathbf{X}^{ij}$ represents the (i, j)th pixel value of image X, and $\|\cdot\|_F$ denotes Frobenius matrix norm. Note that the relative error measure defined in (14) is based on the inverse signal-to-noise ratio (SNR^{-1}) averaged for all the pixels in the image.

Fig. 3 presents a filtering quality comparison, in terms of (14), of the proposed BPT pruning based on the number of regions with the dissimilarity measures defined in Section III. The number of regions n_r is shown in the upper horizontal axis with logarithmic scale. In the lower horizontal axis, the mean region area in pixels is stated, calculated as $(n_h \cdot n_w)/n_r$. The plot also compares the BPT pruning based on the number of regions with the multilook filter (4), for different window sizes. In this case, the mean region size corresponds to the nominal window size, i.e., n in (4). For the BPT-based filtering, an initial 3×3 multilook has been applied in order to get full rank matrices needed for d_{RW} (7) and d_{WR} (8) dissimilarities. The results have been obtained averaging 25 different realizations of the simulated image. For the multilook and the d_{RW} cases, the standard deviation values resulting from the 25 realizations are also included. The rest of the curves present similar values to the d_{RW} case.

When there are variations in intensity, Fig. 3(a) and (c), for small values of region size, the results of the BPT pruning based on the region number are very close to the Boxcar filter, as the region mixture is negligible. For region sizes in the order of 50–100 pixels (equivalent to 9×9 Boxcar filter), the error measure starts to increase rapidly for the Boxcar filter as the region mixture near the contours becomes appreciable. On the contrary, the BPT is able to adapt to the image morphology minimizing this region mixture effect, and thus, the error measure keeps decreasing when the average region size increases, achieving the best error bounds near the four regions which should be the optimum as the simulated image has exactly four different regions.

In Fig. 3(b), the error plots are completely different since only the dissimilarity measures that use all the covariance matrix information are sensitive to the region contours. Therefore, the regions generated using d_{DN} (10), d_{DR} (11), and d_{DW} (12) rapidly start mixing nonhomogeneous regions and never improve the multilook filter performance. On the other hand, full matrix dissimilarities d_{RW} (7) and d_{WR} (8) can adapt to the image morphology and overcome Boxcar error measures

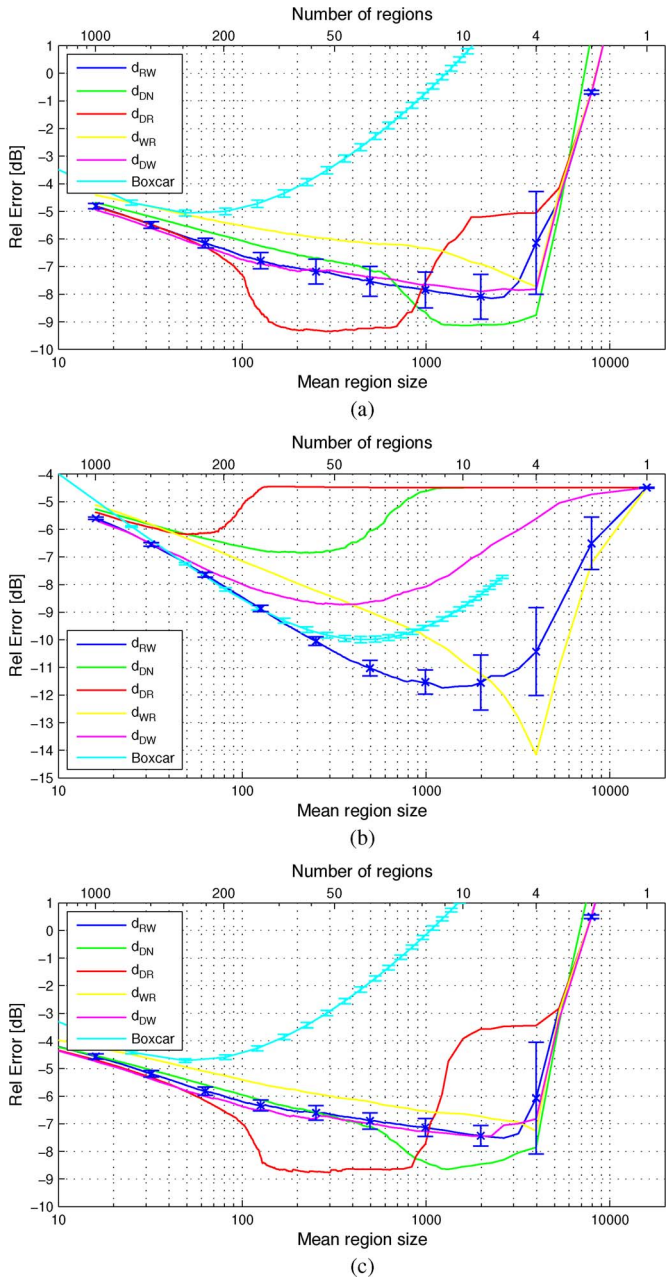

Fig. 3. Relative matrix error for simulated images with four equal size zones filtered with a BPT pruning based on the region number. Results have been obtained averaging 25 realizations. (a) Variation in intensity. (b) Variation in correlation. (c) Variations both in correlation and in intensity.

with higher region sizes. Note that, in Fig. 3(b), the intensity is constant over the entire image. As a result, the mixing of different regions has not a dramatic impact in the relative error as in Fig. 3(a) and (c). This also explains why the minimum of the Boxcar error occurs at region sizes about 400–500 pixels (21×21 multilook filter).

Comparing the different proposed dissimilarity functions, when there are variations in intensity d_{DN} (10) and d_{DR} (11) can achieve better performance in terms of relative error, but the minimum can be far away from the four regions case. Wishart-based dissimilarities, either diagonal d_{DW} (12) or full matrix d_{RW} (7), have very constant and stable behavior when increasing the mean region size and achieve the best results

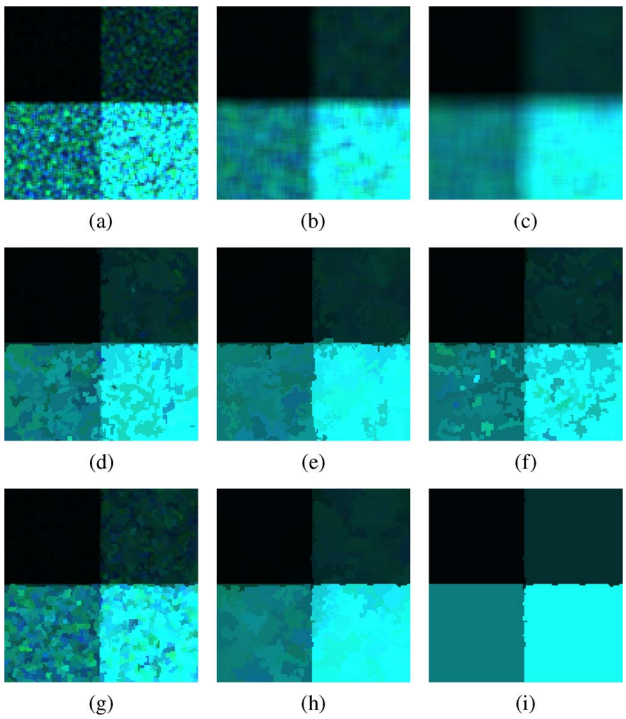

Fig. 4. Boxcar and BPT filtering (pruning based on the region number) in one of the simulated PolSAR images with variations in both correlation and intensity employing different dissimilarity functions. C_{11}, C_{22}, and C_{33} are assigned to blue, red, and green channels, respectively. (a) Boxcar 3×3. (b) Boxcar 9×9. (c) Boxcar 15×15. (d) d_{DN}, $n_r = 100$. (e) d_{DW}, $n_r = 100$. (f) d_{WR}, $n_r = 100$. (g) d_{RW}, $n_r = 1000$. (h) d_{RW}, $n_r = 100$. (i) d_{RW}, $n_r = 4$.

near the point corresponding to four regions. Ward-based dissimilarity d_{WR} (8) can have poor performance when compared with other dissimilarities, but it is the only one that presents a clear minimum always at exactly four regions. At this point, its performance in terms of relative error is comparable to the Wishart-based dissimilarities. When intensity is constant, only full matrix Wishart and Ward dissimilarities can adapt to the image morphology and outperform Boxcar performances. In this case, Ward dissimilarity performance at four regions is near 3 dB better than the Wishart minimum at about ten regions.

Fig. 4 shows the results of applying the pruning based on the number of regions in one realization of the simulated data with variations both in correlation and in intensity compared with Boxcar filtering. As it may be seen in Fig. 4(a)–(c), as the Boxcar filter size increases, the amount of speckle noise reduction and the quality of the estimation increase. However, the spatial resolution is degraded considerably as the filter size increases, blurring completely the region contours. In Fig. 4(d)–(f), the number of regions n_r is fixed to 100, and different dissimilarity measures for BPT construction are compared. All of them are able to detect the main contours of the four zones with this number of regions. The contours detected inside the main regions are completely random, and they are due to the speckle noise present on the image. In Fig. 4(g)–(i), the symmetric revised Wishart dissimilarity measure d_{RW} (7) has been employed and the results are shown for different number of regions. For $n_r = 4$, as it may be observed, there is a good preservation of the spatial resolution, but also of the polarimetric information under the Gaussian hypothesis. A comparison between Figs. 2(c) and 4(i) exhibits that the filtered image is quite close to the ideal one. This similarity is also supported by the fact that the relative error function (14), which is also sensitive to the polarimetric information, presents very low values. As detailed previously, each region is represented by the average covariance matrix which is the MLE under the Gaussian hypothesis [21]. Furthermore, as n_r decreases, the number of contours in the filtered image decreases, reducing the effect of the speckle noise, but new contours never appear.

B. Region Homogeneity-Based Pruning

The previous pruning strategy is very simple since no new criterion nor evaluation is needed for pruning. The same dissimilarity measure employed for the BPT construction is employed for pruning, obtaining the n_r most different regions from the tree. However, it presents some drawbacks when applied to real images:

1) The averaged covariance matrix $\mathbf{Z}$ as a region model is a good representation of the region when it is homogeneous in the Gaussian case, but in the upper nodes of the tree, corresponding to larger regions of the image, this assumption is not true. Therefore, a pruning criterion based only on this model is not good for BPT pruning.
2) The optimum region number is completely dependent on the image structure and also on the employed dissimilarity measure, as seen in Fig. 3. In practical situations, it is almost impossible to fix a priori the optimum number of regions for a given PolSAR image.
3) The proposed dissimilarity functions have a strong dependence with the region sizes, which is needed for a good multi-scale representation within the BPT. However, when employed as a pruning criterion, the obtained segmentation has also this strong dependence. This fact implies that, for example, it is very unlikely to obtain in the same segmentation point scatters and large homogeneous regions.

To solve the mentioned problems, the pruning criterion should not rely exclusively on the region model, and it should be independent of the region size. A new BPT pruning strategy is proposed according to this principle with its pruning criterion focused on a region homogeneity measure ϕ.

The proposed criterion ϕ_R measures the average error produced at representing each region X by its model $\mathbf{Z}_X$:

$$\phi_R(X) = \frac{1}{n_x} \sum_{i=1}^{n_x} \frac{\|\mathbf{X}^i - \mathbf{Z}_X\|^2}{\|\mathbf{Z}_X\|^2} = \frac{1}{n_x \|\mathbf{Z}_X\|^2} \sum_{i=1}^{n_x} \|\mathbf{X}^i - \mathbf{Z}_X\|^2 \tag{15}$$

where $\mathbf{X}^i$ represents the covariance matrix for the ith pixel within region X, and n_x is the number of pixels in X. It can also be interpreted as the mean loss of information that occurs when modeling the region by its estimated covariance matrix (4).

Then, the region homogeneity-based pruning will select from the tree a set of regions Θ corresponding to the largest regions having a homogeneity value below a pruning threshold δ_p. This pruning process can be implemented using a top-down

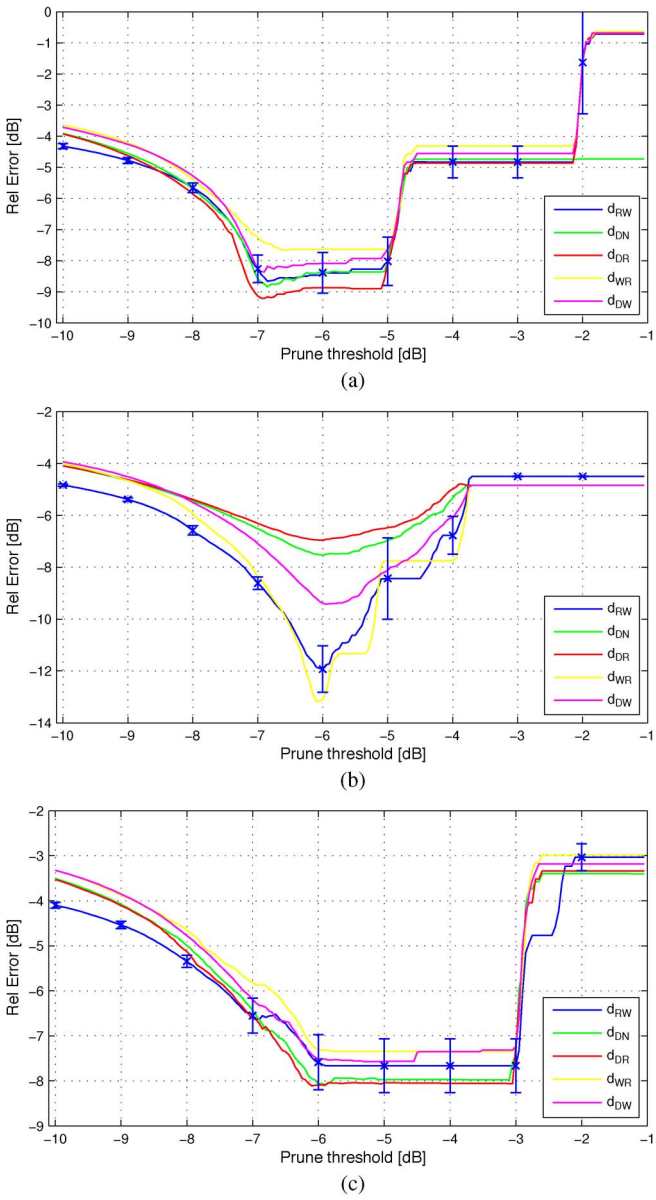

Fig. 5. Relative matrix error for simulated images with four equal size zones filtered with a region homogeneity-based pruning. Results have been obtained averaging 25 realizations. (a) Variation in intensity. (b) Variation in correlation. (c) Variations both in correlation and in intensity.

approach, selecting the first nodes X_i that fulfill the homogeneity criterion $\phi_R(X_i) < \delta_p$. Starting from the root node X_r, it will be checked for homogeneity. If it is not homogeneous, having $\phi_R(X_r) \geq \delta_p$, it will be split into its two child nodes, otherwise it will be added to Θ. Iteratively, each region will be checked for homogeneity and will be split or added to Θ depending on the result. Subsequently, the set of regions Θ will conform a segmentation of the image having a mean information loss below the threshold δ_p for all regions.

This region homogeneity-based pruning has been also evaluated as a PolSAR speckle filtering process with the same simulated images as the pruning based on the number of regions. The results in terms of relative error (14) for different pruning threshold values and dissimilarity measures are shown in Fig. 5. As for the BPT pruning based on the region number, the results have been obtained after averaging 25 different realizations of

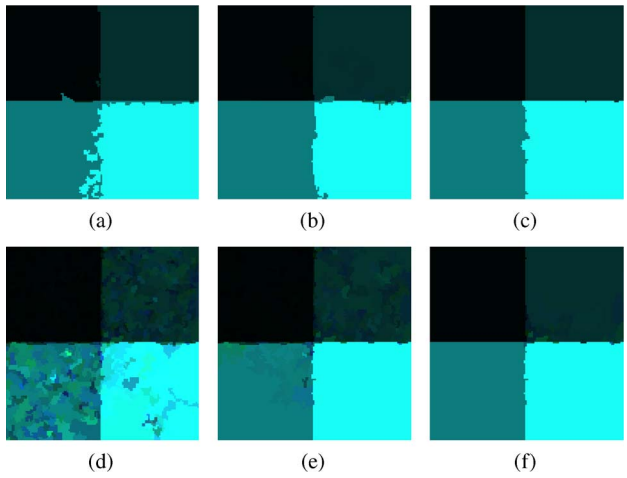

Fig. 6. BPT homogeneity pruning filtering in one of the simulated PolSAR images with variations in both correlation and intensity employing different dissimilarity measures and prune thresholds. C_{11}, C_{22}, and C_{33} are assigned to blue, red, and green channels, respectively. (a) d_{DN}, $\delta_p = -6$ dB. (b) d_{DW}, $\delta_p = -6$ dB. (c) d_{WR}, $\delta_p = -6$ dB. (d) d_{RW}, $\delta_p = -8$ dB. (e) d_{RW}, $\delta_p = -7$ dB. (f) d_{RW}, $\delta_p = -6$ dB.

the simulated image, where the standard deviation values for the d_{RW} distance are included.

As it can be seen in Fig. 5, independent from the image structure, the homogeneity-based pruning behavior versus the prune threshold is very similar for all the dissimilarity measures employed for BPT construction. There is always a minimum in terms of relative error located at the same position. There is also a value for the pruning threshold that is almost optimum for all the images at about -6 dB for δ_p.

When there are variations in intensity, in Fig. 5(a) and (c), a wide set of values for δ_p, ranging from -6 dB to -4 dB or -3 dB, are near optimum. When there are only variations in correlation, as seen in Fig. 5(b), there is not such a wide optimum set of values, but a clear minimum is also located at -6 dB for δ_p.

Comparing Figs. 3 and 5, the minimum values in terms of relative error obtained in BPT pruning based on the number of regions are approximately preserved in the region homogeneity pruning. However, since the homogeneity measure in which pruning is based on is sensitive to all the covariance matrix elements, a small improvement can be observed when the dissimilarity measure is not sensitive to region changes, as seen in Fig. 5(b) for diagonal dissimilarities d_{DN} (10), d_{DR} (11) and d_{DW} (12), which contributes making the homogeneity-based pruning more robust.

Fig. 6 shows the results of applying the BPT homogeneity-based pruning in one realization of the simulated data with variations both in correlation and in intensity. In Fig. 6(a)–(c), the pruning threshold δ_p has been fixed to -6 dB, which is the optimum value for all the simulated images, as seen in Fig. 5. With this pruning threshold, the BPT homogeneity pruning employing all the dissimilarity measures obtain a filtered image very close to the ideal one shown in Fig. 2(c), obtaining a good preservation of the polarimetric information under the Gaussian hypothesis. There are only small differences in the detected contours, which are more accurate for d_{WR} (8) and d_{RW} (7), since they are sensitive to all the covariance matrix information.

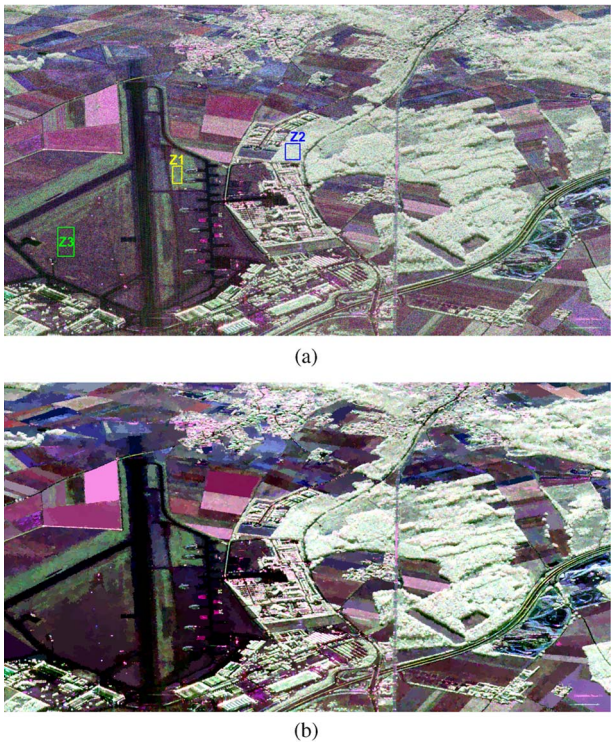

(a)

(b)

Fig. 7. Pauli original image of Oberpfaffenhofen (a) and processed image (b) employing homogeneity-based pruning. RGB channels are assigned to $|hh - vv|$, $|hv + vh|$ and $|hh + vv|$, respectively. Selected homogeneous regions are marked over the original image. (a) Original. (b) d_{RW}, $\delta_p = -2$ dB.

In Fig. 6(d)–(f), the symmetric revised Wishart dissimilarity measure d_{RW} has been employed, and different pruning thresholds are shown. Comparing it with the pruning based on the region number results for the same image, in Fig. 4, they achieve similar results, particularly for high pruning threshold values. Note that the region contours are exactly the same, since the two BPT pruning processes are performed over the same tree.

Nevertheless, the most important properties of this new pruning strategy is to overcome the stated drawbacks of the BPT pruning based on the region number enumerated at the beginning of this section. This advantage can be seen more clearly with real data.

C. Real PolSAR Data Filtering

The BPT-based PolSAR filtering approach has been considered also with real PolSAR data acquired in a measurement campaign conducted by the DLR in 1999 with its experimental E-SAR system, over the Oberpfaffenhofen test-site, southern Germany. Data were collected at L-band, with a spatial resolution of 1.5 m $\times$ 1.5 m in fully polarimetric mode. Fig. 7(a) presents the original Pauli RGB image of the mentioned data set.

The previous data set has been processed with a 7 $\times$ 7 multilook as a reference, the IDAN[1] [4] filter, and the discussed BPT pruning approaches: pruning based on the number of regions and region homogeneity-based pruning. The IDAN approach has been considered in this work as it is very similar to the BPT-based approach, since it considers the selection of an adaptive neighborhood and filters it by assuming a multilook. As indicated by the authors [4], this approach is focused on data filtering, whereas they also introduce an approach based on the linear minimum square error when the focus is on spatial resolution preservation. Fig. 7(b) shows one processed image after applying an homogeneity-based pruning with $\delta_p = -2$ dB over a BPT constructed employing the revised Wishart d_{RW} dissimilarity (7). Fig. 8 shows a detailed area of the image and results after applying the multilook and IDAN filters, whereas Fig. 9 shows the same area processed with different BPT pruning strategies and parameters. The selected area contains some large homogeneous agricultural fields at the top left part of the image and an urban area with small details in the central part. The multilook filter implies a spatial resolution loss. The IDAN filter focuses specifically on data filtering by considering an adaptive neighborhood for every pixel of the data, in opposition to the BPT approach that considers homogeneous regions. As observed, neither the multilook nor the IDAN techniques can achieve such strong filtering as the proposed BPT-based filter. For the BPT construction process, the revised Wishart dissimilarity d_{RW} has been employed. Comparing both pruning criteria, the region homogeneity-based pruning preserves more small details and point targets than the pruning based on the number of regions, as can be seen in urban zones, while, at the same time, it produces larger areas for homogeneous fields. This effect is caused by the strong dependence of the dissimilarity measures with the region sizes, as mentioned before.

(a) (b) (c)

Fig. 8. Detail Pauli RGB images. (a) Original, (b) filtered with 7 $\times$ 7 multilook, and (c) filtered with IDAN.

One of the main features of the BPT is its multi-scale nature, as it has been indicated. This aspect can be deduced from Fig. 9(a)–(f). Note that all of these images have been generated from the same tree, just changing the pruning strategy and parameters. Then, the BPT contains all the information presented in the images at different detail levels. This property is exploited to obtain within the same image strong filtering in case of homogeneous areas whereas the spatial resolution and details of the image are maintained. Decreasing the number of regions n_r or increasing the pruning factor δ_p modifies the strength of the filter, but is worth to notice that new contours never appear, since bigger regions are always generated by fusion of smaller ones. To illustrate the ability of the region homogeneity-based pruning to obtain within the same image regions with very different sizes, Fig. 10 shows a small homogeneous area of the original image with corner reflectors, close to the runway. BPT-based filtering can achieve very strong filtering while preserving the corner reflectors as small spatial details. Multilook and IDAN do not achieve such a strong filtering, and multilook implies a spatial resolution loss, resulting in larger spots.

[1]The PolSARPro [18] IDAN implementation has been employed for this work, with a maximum window size parameter of 100 pixels.

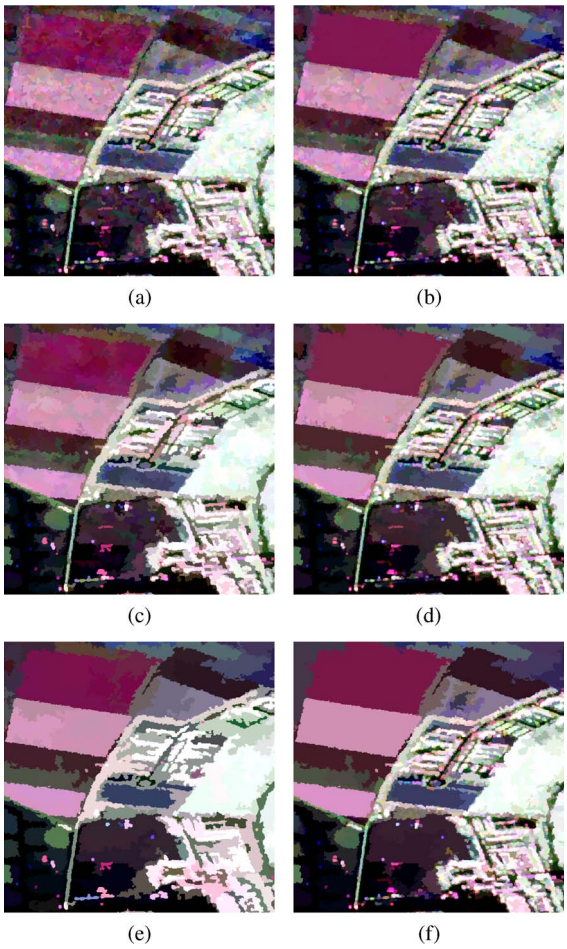

Fig. 9. Detail Pauli RGB images. (a), (c), (e) filtered with pruning based on the number of regions and (b), (d), (f) filtered with region homogeneity-based pruning. (a) d_{RW}, $n_r = 50\,000$. (b) d_{RW}, $\delta_p = -2$ dB. (c) d_{RW}, $n_r = 10\,000$. (d) d_{RW}, $\delta_p = -1$ dB. (d) d_{RW}, $n_r = 2000$. (f) d_{RW}, $\delta_p = 0$ dB.

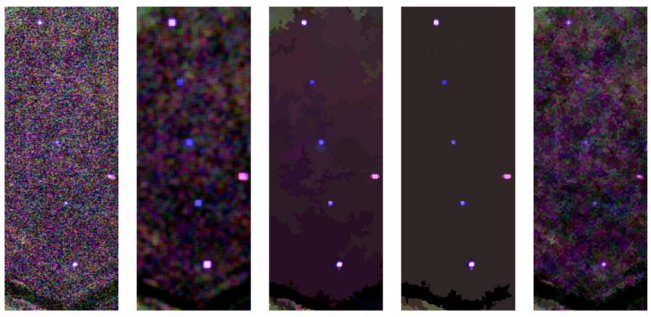

Fig. 10. Detail Pauli RGB images of corner reflectors preservation. For BPT homogeneity-based pruning, the revised Wishart d_{RW} dissimilarity has been employed. For IDAN filter, the maximum window size is 100 pixels. (a) Original. (b) 7×7 ML. (c) $\delta_p = -2$ dB. (d) $\delta_p = 0$ dB. (e) IDAN.

Fig. 9 also shows that the polarimetric information is maintained in the Gaussian case, since the Pauli representations do not vary between the original image Fig. 8(a), and the BPT filtered images. As stated before, the region model employed within the BPT nodes consists of the estimated covariance matrix (4), which represents the MLE of the covariance matrix, assuming a complex Gaussian distribution [21].

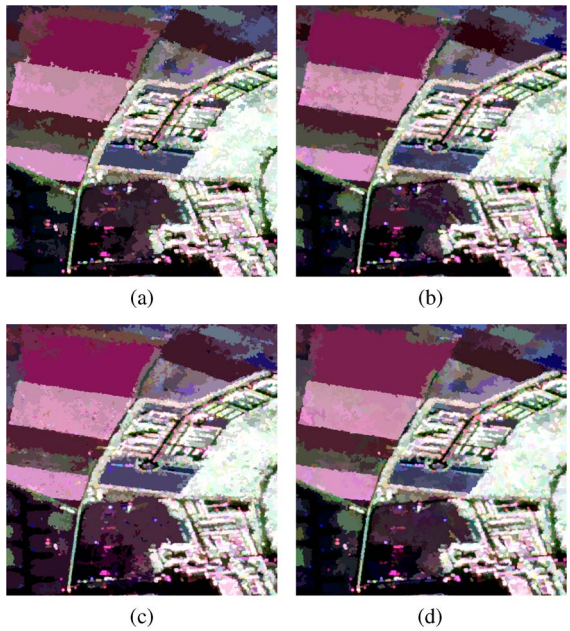

Fig. 11. Detail Pauli RGB images processed using region homogeneity-based pruning with $\delta_p = -1$ dB over different trees constructed employing various dissimilarity functions. (a) d_{WR}, $\delta_p = -1$ dB. (b) d_{DN}, $\delta_p = -1$ dB. (c) d_{DR}, $\delta_p = -1$ dB. (d) d_{DW}, $\delta_p = -1$ dB.

Fig. 11 presents the results for the same image obtained after applying a region homogeneity-based pruning with $\delta_p = -1$ dB over different trees, changing the dissimilarity function employed for the BPT construction process. As one may observe, all the proposed dissimilarity measures are sensitive to the main contours of the image, obtaining large regions over homogeneous areas while preserving contours and small details. However, there are some differences between them. The contours detected employing d_{WR} dissimilarity (8) are noisy [see Fig. 11(a)], as it can be seen particularly in the fields, appearing as a rough line. The BPT obtained with diagonal dissimilarities d_{DN} (10) and d_{DR} (11), Fig. 11(b) and (c), present clear region contours but some small spots can be seen inside homogeneous regions that correspond to the image speckle noise. This effect is more obvious inside the upper fields for d_{DR} dissimilarity. The obtained results with d_{DW} (12), in Fig. 11(d), are very close to the revised Wishart d_{RW} results, shown in Fig. 9(d), since the two dissimilarities are based on the same principles, but some large areas are better characterized with d_{RW}, as it is sensitive to all the covariance matrix elements.

To illustrate the capability to retain the polarimetric information of the proposed BPT filtering approach under the Gaussian hypothesis, the eigendecomposition parameters of the covariance matrix, Entropy (E), Anisotropy (A), and the averaged alpha angle ($\bar{\alpha}$) are shown in Fig. 12 in comparison with the 7×7 multilook and IDAN filtering. An initial qualitative comparison of the images shows that they obtain the same values. However, there are differences for large homogeneous areas in the agricultural fields, where the BPT approach can obtain these parameters with larger filtering than multilook, reducing the estimation errors for distributed scatters. Moreover, in the case of point targets and small details of the image, for example inside the urban areas, it is able to maintain a higher spatial

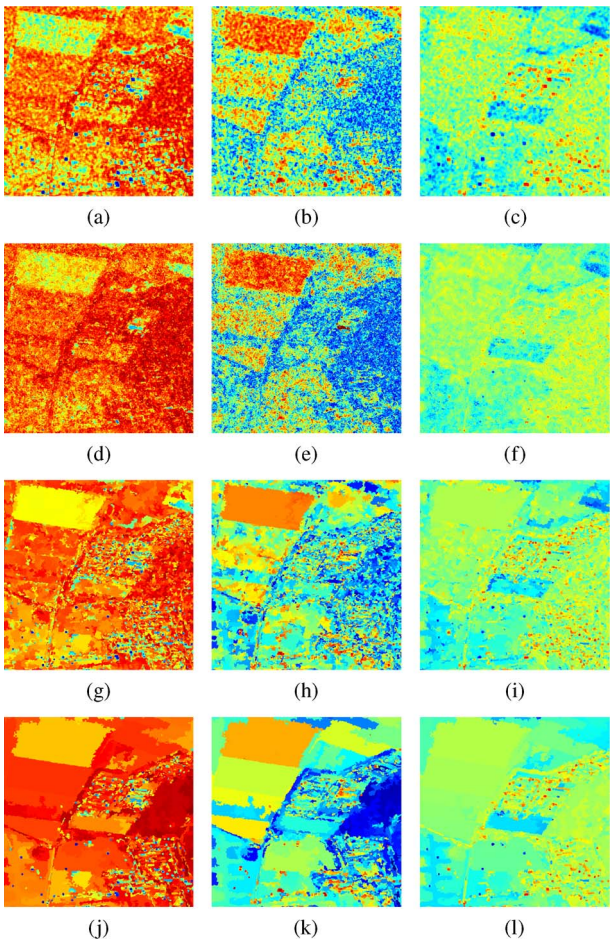

Fig. 12. $H/A/\bar{\alpha}$ from processed images with multilook, IDAN, and using region homogeneity-based pruning for different pruning threshold values and d_{RW} dissimilarity. (a) H, 7×7 multilook. (b) A, 7×7 multilook. (c) $\bar{\alpha}$, 7×7 multilook. (d) H, IDAN. (e) A, IDAN. (f) $\bar{\alpha}$, IDAN. (g) H, $\delta_p = -2$ dB. (h) A, $\delta_p = -2$ dB. (i) $\bar{\alpha}$, $\delta_p = -2$ dB. (j) H, $\delta_p = 0$ dB. (k) A, $\delta_p = 0$ dB. (l) $\bar{\alpha}$, $\delta_p = 0$ dB.

resolution, since smaller regions of the tree are obtained. As a consequence, the proposed BPT filtering approach improves the estimation of the polarimetric information, both, in point as well as in distributed scatters.

To be able to make a quantitative evaluation of the polarimetric information preservation, three homogeneous areas from the image have been selected, and some mean estimated parameters are calculated over them, regarding the covariance matrix elements and the eigendecomposition parameters $H/A/\bar{\alpha}$. The selected areas are shown in Fig. 7(a), and the mean estimated values are presented in Table I. A comparison is made between the original values, 7×7 multilook, IDAN filtering, and BPT homogeneity-based pruning for different δ_p. As it can be seen, in the case of multilook and BPT filtering, the estimated covariance matrix elements are very similar to the original values. However, IDAN filtering introduces appreciable bias in the covariance matrix elements although the eigendecomposition parameters $H/A/\bar{\alpha}$ are close to the other filtering values. The presence of this bias has been discussed in [19] and compensates up to a certain point by the authors [20]. With BPT-based filter and $\delta_p = 0$ dB, the values start to diverge from the original ones because of the inhomogeneous region mixture effect due to excessive filtering. The $H/A/\bar{\alpha}$ parameters cannot be estimated over the original image since its estimated covariance matrices are singular, and then a filtering process is needed. Note that these estimated parameters are biased [6]; increasing the pruning factor means increasing the filtering and the number of looks per region and then reducing the estimation biases for all the eigendecomposition parameters. As expected, as the number of looks increases, the bias is reduced and the estimated entropy increases while anisotropy is reduced.

V. BPT Pruning for Coastline Detection

In Section IV, the BPT representation of the image has been employed for PolSAR filtering. However, the BPT structure contains a lot of useful information about image structure that may be employed for other applications. Fig. 13 is an example where the BPT is employed to obtain an image segmentation over the coastline. Fig. 13(a) shows a 1500 $\times$ 2500-pixel cut of a C-band Pauli RADARSAT-2 image of Barcelona, Spain, that was acquired in November 18th, 2008, in fine quad polarization mode, with nominal resolution of 5.2 m $\times$ 7.6 m. The figure also shows a detailed area corresponding to the Forum harbor of Barcelona. Fig. 13(b) shows two regions of the BPT corresponding to land and sea. In this case, the two most different regions (that is the two child nodes of the root node) were selected. Note that, for coastline detection, upper nodes of the tree, closer to the root, are selected, in opposition to the filtering application, where lower nodes of the tree, closer to the leaves, are interesting. It is worth to notice that, due to the ability of the BPT to preserve small details, the thin structures in the coastline like breakwaters are preserved.

VI. Conclusion

A new PolSAR data processing approach, based on a BPT image representation is presented. The BPT contains a large number of regions that may be extracted from the data, that are organized in a hierarchical structure, corresponding to different scales or detail levels. Consequently, this data representation contains a lot of useful information related to data structure. Thus, the BPT is a powerful tool for developing nonlinear, region-based, and multi-scale PolSAR applications.

The BPT construction process has been analyzed, employing a bottom-up approach. In this case, a region model and a dissimilarity measure need to be defined. The estimated covariance matrix has been selected as a region model, assuming a complex Gaussian model, and different dissimilarity measures have been proposed and analyzed. It is worth to notice that this construction process employs all the elements of the covariance matrix and then exploits all the polarimetric information. Nevertheless, other region models accounting, for instance, for data texture or characterizing high resolution data are possible. The BPT is a general representation of the data, which construction process should be application independent, conforming a common part for all the BPT-based applications.

The processing of the BPT typically involves the identification of the tree nodes that are useful for a particular application. The main application considered in this work is PolSAR

TABLE I
MEAN ESTIMATED VALUES OVER HOMOGENEOUS AREAS FOR DIFFERENT FILTERING STRATEGIES

Region	Filtering	C_{11}	C_{22}	C_{33}	$\Re(C_{13})$	$\Im(C_{13})$	H	A	$\bar{\alpha}$
Z1 5000 px	Original	28.27	16.06	18.34	5.242	5.504	-	-	-
	ML 7x7	28.21	15.97	18.36	5.321	5.465	0.8012	0.3543	48.29
	IDAN	18.73	9.661	12.03	2.471	2.595	0.8558	0.3050	49.48
	BPT -2dB	28.15	16.10	18.17	5.466	5.605	0.8271	0.2873	48.27
	BPT -1dB	28.20	15.20	18.08	5.558	5.612	0.8618	0.2036	47.91
	BPT 0dB	27.76	14.47	16.96	5.813	5.211	0.8694	0.1630	47.74
Z2 5950 px	Original	279.3	159.1	172.8	49.80	-14.37	-	-	-
	ML 7x7	280.8	159.3	172.9	49.18	-15.27	0.8598	0.2907	49.06
	IDAN	173.0	102.4	105.8	20.59	-7.978	0.9003	0.2501	51.29
	BPT -2dB	278.1	158.4	171.5	48.05	-16.12	0.8475	0.2984	49.50
	BPT -1dB	280.4	157.7	172.4	50.24	-15.42	0.8925	0.2269	49.41
	BPT 0dB	292.2	160.8	177.0	50.74	-13.42	0.9305	0.1307	49.61
Z3 18000 px	Original	10.70	2.782	13.13	2.644	5.599	-	-	-
	ML 7x7	10.70	2.789	13.14	2.662	5.593	0.6781	0.4248	42.62
	IDAN	7.123	1.864	8.678	1.433	2.896	0.7438	0.4505	44.39
	BPT -2dB	10.33	2.713	12.94	2.498	5.255	0.7370	0.3755	43.32
	BPT -1dB	10.36	2.799	13.23	2.434	5.136	0.7445	0.3881	43.60
	BPT 0dB	11.76	3.405	13.59	2.556	5.351	0.7852	0.3471	44.34

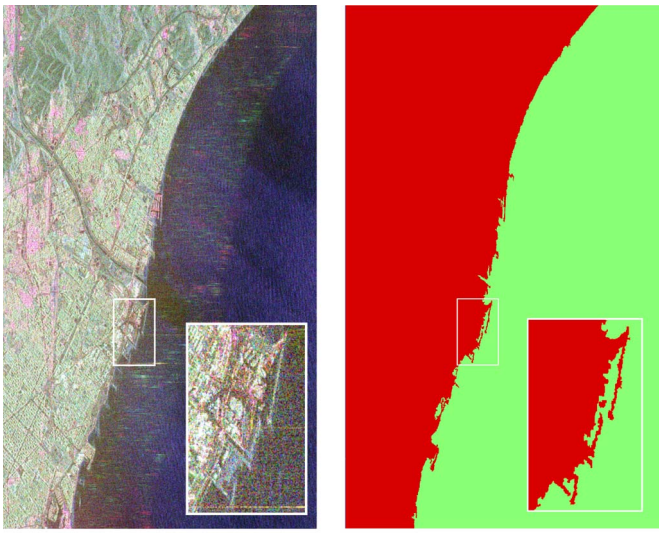

(a) (b)

Fig. 13. (a) Pauli RGB image of Barcelona, and (b) coastline segmentation with BPT. The revised Wishart d_{RW} dissimilarity has been employed for the BPT construction.

speckle filtering. The target for speckle filtering application is to detect the largest homogeneous regions within the image. Two tree pruning strategies for the filtering application have been proposed, the pruning based on the number of regions and the homogeneity-based pruning. The proposed BPT-based PolSAR speckle filtering process has shown to achieve very high level of noise filtering while preserving small details and spatial resolution. Furthermore, the proposed technique is able to exploit all the polarimetric information under the Gaussian assumption, unlike most state-of-the-art filtering techniques, that are only based on radiometric information. The number of regions n_r or the pruning factor δ_p may be employed to adjust the strength of the filtering. Additionally, it has been observed that no bias or distortion is introduced in the polarimetric information as the region model that has been employed, the average covariance or coherency matrices, corresponds to the MLE of these matrices.

Secondarily, another BPT-based application of PolSAR data processing is presented: coastline detection. In this case, the goal is to detect the two most different regions corresponding to sea and land and then identify the coastline as their contour. Due to the ability of the BPT to preserve small details and spatial resolution, this coastline detection can detect thin structures in the coastline like breakwaters.

ACKNOWLEDGMENT

The authors would like to thank DLR and MDA for providing the ESAR and the RADARSAT-2 data sets, respectively. The authors would like also to acknowledge the reviewers for their valuable comments and Dr. Jordi Mallorquí for his support in the development of this work.

REFERENCES

[1] A. B. Kostinski and W. M. Boerner, "On foundations of radar polarimetry," *IEEE Trans. Antennas Propag.*, vol. AP-34, no. 12, pp. 1395–1404, Dec. 1986.
[2] S. Cloude and E. Pottier, "A review of target decomposition theorems in radar polarimetry," *IEEE Trans. Geosci. Remote Sens.*, vol. 34, no. 2, pp. 498–518, Mar. 1996.
[3] J.-S. Lee, M. Grunes, and G. de Grandi, "Polarimetric SAR speckle filtering and its implication for classification," *IEEE Trans. Geosci. Remote Sens.*, vol. 37, no. 5, pp. 2363–2373, Sep. 1999.
[4] G. Vasile, E. Trouve, J.-S. Lee, and V. Buzuloiu, "Intensity-driven adaptive-neighborhood technique for polarimetric and interferometric SAR parameters estimation," *IEEE Trans. Geosci. Remote Sens.*, vol. 44, no. 6, pp. 1609–1621, Jun. 2006.
[5] C. López-Martínez and X. Fàbregas, "Model-based polarimetric SAR speckle filter," *IEEE Trans. Geosci. Remote Sens.*, vol. 46, no. 11, pp. 3894–3907, Nov. 2008.
[6] C. López-Martínez, E. Pottier, and S. Cloude, "Statistical assessment of eigenvector-based target decomposition theorems in radar polarimetry," *IEEE Trans. Geosci. Remote Sens.*, vol. 43, no. 9, pp. 2058–2074, Sep. 2005.
[7] P. Salembier and L. Garrido, "Binary partition tree as an efficient representation for image processing, segmentation and information retrieval," *IEEE Trans. Image Process.*, vol. 9, no. 4, pp. 561–576, Apr. 2000.
[8] J. W. Goodman, "Some fundamental properties of speckle," *J. Opt. Soc. Amer.*, vol. 66, no. 11, pp. 1145–1149, Nov. 1976.
[9] N. R. Goodman, "Statistical analysis based on a certain multivariate complex Gaussian distribution (an introduction)," *Ann. Math. Statist.*, vol. 34, no. 1, pp. 152–177, Mar. 1963.

[10] R. J. A. Tough, D. Blacknell, and S. Quegan, "A statistical description of polarimetric and interferometric synthetic aperture radar data," *Proc. R. Soc. Lond. A, Math. Phys. Sci.*, vol. 449, no. 1937, pp. 567–589, Jun. 1995.
[11] J.-S. Lee, K. Hoppel, S. Mango, and A. Miller, "Intensity and phase statistics of multilook polarimetric and interferometric SAR imagery," *IEEE Trans. Geosci. Remote Sens.*, vol. 32, no. 5, pp. 1017–1028, Sep. 1994.
[12] O. Morris, M. Lee, and A. Constantinidies, "Graph theory for image analysis: An approach based on the shortest spanning tree," *Proc. Inst. Elect. Eng.—F*, vol. 133, no. 2, pp. 146–152, Apr. 1986.
[13] L. Garrido, P. Salembier, and D. Garcia, "Extensive operators in partition lattices for image sequence analysis," *Signal Process.*, vol. 66, no. 2, pp. 157–180, Apr. 1998.
[14] L. M. Novak and M. C. Burl, "Optimal speckle reduction in polarimetric SAR imagery," *IEEE Trans. Aerosp. Electron. Syst.*, vol. 26, no. 2, pp. 293–305, Mar. 1990.
[15] P. R. Kersten, J.-S. Lee, and T. L. Ainsworth, "Unsupervised classification of polarimetric synthetic aperture radar images using fuzzy clustering and EM clustering," *IEEE Trans. Geosci. Remote Sens.*, vol. 43, no. 3, pp. 519–527, Mar. 2005.
[16] J. H. Ward, "Hierarchical grouping to optimize an objective function," *J. Amer. Stat. Assoc.*, vol. 58, no. 301, pp. 236–244, Mar. 1963.
[17] S. Normann, R. Jenssen, and T. Eltoft, "Spectral clustering of polarimetric SAR data with Wishart-derived distance measures, in *Proc. PolInSAR*, Jan. 2007. [Online]. Available: http://earth.esa.int/workshops/polinsar2007/papers/140_anfinsen.pdf
[18] PolSARPro v. 4.0.3. [Online]. Available: http://earth.esa.int/polsarpro
[19] G. Vasile, J.-P. Ovarlez, F. Pascal, and C. Tison, "Coherency matrix estimation of heterogeneous clutter in high-resolution polarimetric SAR images," *IEEE Trans. Geosci. Remote Sens.*, vol. 48, no. 4, pp. 1809–1826, Apr. 2010.
[20] G. Vasile, J.-P. Ovarlez, F. Pascal, C. Tison, L. Bombrun, M. Gay, and E. Trouv, "Normalized coherency matrix estimation under the SIRV model—Alpine glacier POLSAR data analysis," in *Proc. IEEE IGARSS*, Boston, MA, Jul. 2008, vol. 1, pp. I74–I77.
[21] R. J. Muirhead, *Aspects of Multivariate Statistical Theory*. New York: Wiley, 1982.
[22] A. Alonso-González, C. López-Martínez, and P. Salembier, "Filtering and segmentation of polarimetric SAR images with Binary Partition Trees," in *Proc. IEEE IGARSS*, Honolulu, HI, Jul. 2010, pp. 4043–4046.

Alberto Alonso-González was born in León, Spain, in 1984. He received the B.Sc. degree in computer science and the M.Sc. degree in telecommunication engineering from the Technical University of Catalonia (UPC), Barcelona, Spain, in 2007 and 2009, respectively, where he is currently working toward the Ph.D. degree in telecommunication engineering. His Ph.D. thesis is focused on multidimensional SAR data modeling and processing.

In 2009, he joined the Signal Theory and Communications Department (TSC), UPC. His research interests include multidimensional SAR, SAR interferometry and polarimetry, digital signal and image processing, and data segmentation and simplification techniques.

Carlos López-Martínez (S'97–M'04–SM'11) received the M.Sc. degree in electrical engineering and the Ph.D. degree from the Universitat Politècnica de Catalunya, Barcelona, Spain, in 1999 and 2003, respectively.

From October 2000 to March 2002, he was with the Frequency and Radar Systems Department, HR, German Aerospace Center, DLR, Oberpfaffenhofen, Germany. From June 2003 to December 2005, he has been with the Image and Remote Sensing Group—SAPHIR Team, in the Institute of Electronics and Telecommunications of Rennes (I.E.T.R—CNRS UMR 6164), Rennes, France. In January 2006, he joined the Universitat Poltècnica de Catalunya as a Ramón-y-Cajal researcher, Barcelona, Spain, where he is currently associate professor in the area of remote sensing and microwave technology. His research interests include SAR and multidimensional SAR, radar polarimetry, physical parameter inversion, digital signal processing, estimation theory and harmonic analysis.

Dr. López-Martínez served as Guest Editor of the *EURASIP Journal on Advances in Signal Processing*. He has organized different invited sessions in international conferences on radar and SAR polarimetry. He has presented advanced courses and seminars on radar polarimetry to a wide range of organizations and events. He received the Student Prize Paper Award at the EUSAR 2002 Conference, Cologne, Germany.

Philippe Salembier (M'96–SM'09–F'11) received the degree from the Ecole Polytechnique, Paris, France, in 1983, the degree from the Ecole Nationale Supérieure des Télécommunications, Paris, France, in 1985, and the Ph.D. degree from the Swiss Federal Institute of Technology (EPFL), Zurich, Switzerland, in 1991. He was a Postdoctoral Fellow at the Harvard Robotics Laboratory, Cambridge, MA, in 1991. He is a Fellow of the IEEE.

From 1985 to 1989, he worked at Laboratoires d'Electronique Philips, Limeil-Brevannes, France, in the fields of digital communications and signal processing for HDTV. In 1989, he joined the Signal Processing Laboratory of the Swiss Federal Institute of Technology in Lausanne, Switzerland, to work on image processing. At the end of 1991, after a stay at the Harvard Robotics Laboratory, he joined the Technical University of Catalonia, Barcelona, Spain, where he is currently professor lecturing on the area of digital signal and image processing. His research interests include image and video sequence analysis, coding and indexing, mathematical morphology, level sets, and nonlinear filtering. In terms of standardization activities, he has been particularly involved in the definition of the MPEG-7 standard ("Multimedia Content Description Interface") as chair of the "Multimedia Description Scheme" group between 1999 and 2001.

Dr. Salembier was member of the Image and Multidimensional Signal Processing Technical Committee of the IEEE Signal Processing Society between 2000–2006 and was technical chair (with Prof. Ed. Delp) of the 2003 IEEE International Conference on Image Processing, organized in Barcelona. He served as Associate Editor of the IEEE TRANSACTIONS ON IMAGE PROCESSING between 2002 and 2008 and of the IEEE SIGNAL PROCESSING LETTERS between 2005 and 2008. He served as an Area Editor of the *Journal of Visual Communication and Image Representation* (Academic Press) from 1995 until 1998 and as an AdCom officer of the European Association for Signal Processing (EURASIP) from 1994 until 1999. He has edited special issues of Signal Processing on "Mathematical Morphology" (1994) and on "Video sequence analysis" (1998). He has also coedited (with Prof. Fernando Pereira) a special issue of Signal processing: Image Communication on MPEG-7 Technology (2000). He was Coeditor-in-Chief of Signal Processing between 2001 and 2002. Finally, he is currently serving as Associate Editor of the *Eurasip Journal on Image and Video Processing*, *Elsevier Signal Processing: Image Communication* and the IEEE TRANSACTIONS ON CIRCUITS AND SYSTEMS FOR VIDEO TECHNOLOGY.